Human Brain Mapping

WILEY

RESEARCH ARTICLE OPEN ACCESS

Dynamic and Static Structure–Function Coupling With Machine Learning for the Early Detection of Alzheimer's Disease

Han Wu[1] | Yinping Lu[2] | Luyao Wang[3] | Jinglong Wu[2] | Ying Liu[1] | Zhilin Zhang[2]

[1]School of Software, Northeastern University, Shenyang, China | [2]Research Center for Medical Artificial Intelligence, Shenzhen Institute of Advanced Technology, Chinese Academy of Sciences, Shenzhen, Guangdong, China | [3]Institute of Biomedical Engineering, School of Life Sciences, Shanghai University, Shanghai, China

Correspondence: Luyao Wang (wangly1018@shu.edu.cn) | Zhilin Zhang (zhangzhilin@siat.ac.cn)

Received: 18 December 2024 | **Revised:** 5 March 2025 | **Accepted:** 13 March 2025

Funding: This work was supported by GuangDong Basic and Applied Basic Research Foundation, 2023A1515012929, Science and Technology Planning Project of Guangdong Province, China, 2023A0505050162.

Keywords: Alzheimer's disease | dynamic structure–function coupling | machine learning | magnetic resonance imaging | static structure–function coupling

ABSTRACT

The progression of Alzheimer's disease (AD) involves complex changes in brain structure and function that are driven by their interaction, making structure–function coupling (SFC) a valuable indicator for early detection of AD. Static SFC refers to the overall structure–function interaction, whereas dynamic SFC refers to transient coupling variations. In this study, we aimed to assess the potential of combining static and dynamic SFC with machine learning (ML) for the early detection of AD. We analyzed a discovery cohort and an external validation cohort, including AD, mild cognitive impairment (MCI), and healthy control (HC) groups. Then, we quantified differences between static SFC and dynamic SFC at different stages of AD progression. Feature selection was performed using ElasticNet. A Gaussian naive Bayes (GNB) classifier was used to test the ability of SFC to classify AD stages. We also analyzed the correlations between SFC features and early AD physiological biomarkers. Static SFC increased with AD progression, whereas dynamic SFC showed greater variability and decreased stability. Using SFC features selected by ElasticNet, the GNB classifier achieved high performance in differentiating between the HC and MCI stages (area under the curve [AUC] = 91.1%) and between the MCI and AD stages (AUC = 89.03%). Significant correlations were found between SFC features and physiological biomarkers. The combined use of SFC features and ML has strong potential value for the accurate classification of AD stages and significant potential value for the early detection of AD. This study demonstrates that combining static and dynamic SFC with ML provides a novel perspective for understanding the mechanisms of AD and contributes to improving its early detection.

1 | Introduction

Alzheimer's disease (AD) is a progressive neurological disorder that leads to the deterioration of cognitive ability and has no definitive cure once diagnosed (Frizzell et al. 2022; Jack Jr. et al. 2018). Early detection, particularly during its prodromal stage known as mild cognitive impairment (MCI), is crucial because it provides an opportunity to implement timely intervention and slow disease progression (Liu et al. 2024; Rasmussen and Langerman 2019). At the MCI stage, structural connectivity (SC) experiences abnormal disruptions, and the strength of functional connectivity (FC) begins to decline;

both values worsen in the AD stage (Cha et al. 2013; Chen et al. 2023; Grieder et al. 2018; Wang et al. 2021). However, structural and functional changes in the brain are not independent. Neuroimaging studies have shown that the anatomical structure constrains and partly determines FC and neuronal activity (Honey et al. 2010; Sun et al. 2014). Conversely, FC shapes SC through neuromodulation and neuroplasticity processes (Batista-García-Ramó and Fernández-Verdecia 2018; Palop and Mucke 2016). The interaction between SC and FC amplifies subtle pathological changes; therefore, the combination of SC and FC performs better in the detection of AD than SC or FC alone does (Collin et al. 2017; Demirtaş et al. 2017; Jiang et al. 2019; Zhang et al. 2017).

Structure–function coupling (SFC) refers to the relationship between SC and FC in the brain (Baum et al. 2020). SFC can be divided into static and dynamic SFC. Static SFC refers to the steady relationship between structure and function throughout the entire scan, which reflects the overall structure–function relationship (Vázquez-Rodríguez et al. 2019). In contrast, dynamic SFC represents the time-varying relationship between SC and FC. Unlike static SFC, dynamic SFC measures coupling variation within a time slice of the scanning session and can reveal transient characteristics of structure–function relationships that might be averaged out in static SFC (Liu, Vázquez-Rodríguez, et al. 2022). In short, static SFC represents the overall structure–function relationship, whereas dynamic SFC represents the variability of that relationship.

Previous studies have focused mainly on static SFC and indicated that static SFC increases as AD progresses but is unable to capture the time-varying nature of dynamic SFC (Cao et al. 2020; Dai et al. 2019; Zhang et al. 2017). The primary limitation of static SFC studies is their insensitivity to temporal order, meaning that they provide only a snapshot of SFC at a specific moment, potentially overlooking critical temporal fluctuations in the relationship between SC and FC. These fluctuations may be essential for understanding the subtle changes in cortical hierarchies and topological and geometric embedding in AD (Liu, Vázquez-Rodríguez, et al. 2022; Liu, Wang, et al. 2022). Therefore, combining static and dynamic SFC allows us to better understand overall and transient abnormalities in SC and FC and to carefully capture distinct and meaningful SFC patterns during adaptation or deterioration as AD progresses.

Machine learning (ML) has emerged as a transformative technology in the field of medical imaging, revolutionizing diagnostic processes and improving clinical decision-making (Mirzaei and Adeli 2022). Feature selection and classifier training are two core components of ML. ElasticNet is a classical feature selection method that combines the strengths of least absolute shrinkage and selection operator (LASSO) and ridge regression. This module uses L1 regularization to prioritize features that are most relevant to the target, whereas L2 regularization addresses multicollinearity issues (Zou and Hastie 2005). This combination makes ElasticNet particularly suitable for high-dimensional magnetic resonance imaging (MRI) data, as it effectively filters out noisy features. Consequently, ElasticNet improves both analysis stability and prediction accuracy in MRI tasks (Wu et al. 2022; Xiao et al. 2021). The Gaussian naive Bayes (GNB) algorithm serves as a probabilistic classifier commonly used in neuroimaging. GNB is based on Bayes' theorem, which assumes conditional independence among features and models each feature using a Gaussian distribution (Anand et al. 2022). This approach enables GNB to manage the complex features in MRI data efficiently, computing conditional probabilities for each class. By optimizing feature selection and reducing redundancy, GNB achieves high-speed, accurate classification in MRI analysis (Madhusudhana et al. 2020). Our hypothesis is that using static and dynamic SFC as features, combined with ElasticNet for feature selection, may improve classification accuracy.

The aim of this study was to investigate whether SFC, when combined with ML methods, can be used to effectively classify different stages of AD. (1) We first calculated both the static and dynamic SFC for all subjects to explore the interaction of structure–function changes throughout AD progression. (2) Next, we combined SFC features with ML methods to evaluate their performance in distinguishing between the HC and MCI stages and between the MCI and AD stages. (3) We then analyzed the SFC features to understand their distribution across brain regions and how they change in different AD stages. (4) Finally, we examined the correlation between these SFC features and physiological biomarkers to assess their potential to reflect early pathological changes associated with AD.

2 | Materials and Methods

2.1 | Participants

Data were obtained from two sources: the Alzheimer's Disease Neuroimaging Initiative (ADNI) (http://www.adni-info.org), which served as the discovery cohort, and the First Hospital of Jilin University, China, which served as the external validation cohort (Table S1). Baseline MRI scans were collected from the ADNI database for 221 participants, comprising 40 AD patients, 94 MCI patients, and 87 healthy controls (HCs). The First Hospital of Jilin University contributed data from 94 participants, including 29 AD patients, 33 MCI patients, and 32 HCs. All procedures were conducted in accordance with the Helsinki Declaration. The inclusion criteria for participants in this study were as follows: aged between 55 and 85 years and a minimum of 6 years of formal education. There were no restrictions with regard to sex. The participants were required to have no history of neurological or psychiatric disorders. Prior to the experiment, all participants provided written informed consent before the experiment and participated in cognitive psychological evaluations, including the Mini-Mental State Examination (MMSE), Montreal Cognitive Assessment (MoCA) and Clinical Dementia Rating Scale (CDR) (Morris 1993). Using the scale information, the diagnosis and enrollment of the participants were performed by experienced clinical neurologists. Additionally, participants with a history of stroke, psychiatric disorders, substance abuse, severe hypertension, systemic diseases, or intellectual disabilities were excluded. Similar criteria were applied to the external validation cohort to ensure the consistency and comparability of the data across all groups (Zheng et al. 2019).

ADNI participants, sourced from multiple centers and encompassing a diverse range of ethnicities, were scanned using three scanners: a Philips 3 T MRI scanner, a GE 3 T MRI scanner, and

TABLE 1 | Demographic information of ADNI cohort and external validation cohort.

Discovery cohort				
	AD	**MCI**	**HC**	***p***
Male/female	15/25	41/53	41/46	0.60[a]
Age	73.56 ± 5.89	72.31 ± 6.93	71.61 ± 6.93	0.28[b]
Education	15.85 ± 2.19	16.36 ± 2.57	16.53 ± 2.53	0.36[b]
MMSE	21.08 ± 3.53	27.29 ± 2.48	29.14 ± 1.14	< 0.001*[b]
MoCA	14.83 ± 4.09	22.30 ± 3.23	27.26 ± 1.87	< 0.001*[b]
External validation cohort				
	AD	**MCI**	**HC**	***p***
Male/female	11/18	12/20	13/19	0.94[a]
Age	66.99 ± 7.60	65.16 ± 8.11	62.85 ± 6.99	0.11[b]
Education	8.97 ± 4.37	9.52 ± 3.49	9.93 ± 2.37	0.55[b]
MMSE	15.66 ± 6.48	24.09 ± 3.63	28.97 ± 1.45	< 0.001*[b]
MoCA	12.00 ± 6.19	18.67 ± 3.84	27.09 ± 1.97	< 0.001*[b]

Note: Data are shown as the mean ± standard deviation (SD).
[a]Denotes the χ^2 test.
[b]Denotes one-way analysis of variance (ANOVA).
*Denotes significance.

a Siemens 3 T MRI scanner. Structural diffusion tensor imaging (DTI) data, T1-weighted (T1W) data, and functional MRI (fMRI) data were collected from all participants. Notably, we included only fMRI data with a repetition time (TR) of 3 s. After preprocessing corrections, all DTI, T1W, and fMRI scans underwent quality assurance checks to exclude scans with excessive motion and/or artifacts; all scans were included.

Participants recruited from the First Hospital of Jilin University were scanned using a 3 T field strength Siemens MRI scanner equipped with a standard head coil. Prior to the scan, the participants were instructed to keep their eyes closed and remain awake during the acquisition process. MR images, including both T1W and resting-state fMRI scans, were obtained. The fMRI parameters were as follows: TR = 3000 ms, echo time (TE) = 27 ms, flip angle = 90°, and field of view (FOV) = 230 × 230 mm. The T1W parameters were as follows: TR = 8.5 ms, TE = 3.3 ms, flip angle = 12°, and FOV = 256 × 256 mm. The DTI parameters were as follows: TR = 8000 ms, TE = 97 ms, flip angle = 90°, and FOV = 256 × 133 mm.

Detailed demographic information is presented in Table 1. In both the discovery cohort and the external validation cohort, there were no significant differences in sex, age, or years of education among the AD, MCI, and HC groups (all p values > 0.05). As expected, scores on the MMSE and MoCA significantly decreased as AD progressed.

2.2 | Data Preprocessing

Preprocessing of DTI data was performed using the PANDA toolbox (Cui et al. 2013). DICOM files were converted to the NIfTI format, and a brain mask was generated to exclude nonbrain tissue. Eddy current distortion and head motion corrections were applied to the diffusion-weighted images, which were then registered to the b0 reference image. The corrected DTI data were aligned with T1W images to ensure spatial consistency.

fMRI scans were preprocessed using fMRIprep (Esteban et al. 2019). The first 10 time points were discarded to mitigate signal inhomogeneity. Motion correction was performed using the Linear Registration Tool in FMRIB (MCFLIRT), followed by slice-timing correction. Each subject's functional images were registered to the corresponding T1W structural image and normalized to Montreal Neurological Institute (MNI) space using FLIRT and FNIRT. Spatial smoothing was performed with a full width at half maximum (FWHM) Gaussian kernel of 6 mm. Linear detrending and bandpass filtering (0.01–0.08 Hz) were used to remove slow signal drifts and retain the desired frequency range. Six rigid-body motion parameters, as well as white matter and cerebrospinal fluid signals, were regressed out to minimize noise from nonneuronal sources. Finally, the nilearn.signal.clean_image function was used to standardize the data, yielding normalized blood oxygen level-dependent (BOLD) time series data for further analysis.

2.3 | Network Construction

To construct the SC network, we employed Bayesian estimation of diffusion parameters obtained by sampling techniques and probabilistic tractography with crossing fibers. The following parameters were applied: 5000 samples per voxel, a curvature threshold of 0.2, a step length of 0.5 mm, and 2000 steps per sample. The SC matrix was generated by calculating the number of probabilistic streamlines passing through 400 brain regions defined by the Schaefer400 atlas (Schaefer et al. 2018).

For the static FC network, Pearson correlation coefficients were calculated for each pair of 400 brain regions using the BOLD time series, as follows:

$$r_{ij} = \frac{\sum_{t=1}^{T}\left(X_i(t)-\overline{X_i}\right)\left(X_j(t)-\overline{X_j}\right)}{\sqrt{\sum_{t=1}^{T}\left(X_i(t)-\overline{X_i}\right)^2\sum_{t=1}^{T}\left(X_j(t)-\overline{X_j}\right)^2}} \quad (1)$$

where $X_i(t)$ and $X_j(t)$ represent the BOLD signal intensities of regions i and j at time point t, respectively; $\overline{X_i}$ and $\overline{X_j}$ represent the mean BOLD signals for these regions, and is the length of the time series (Dai et al. 2019). These coefficients were then transformed using Fisher's z-transformation, resulting in the FC matrix. In this network, the nodes represented brain regions, whereas the edges reflected the strength of the FC between those regions.

For the dynamic FC network, both a time cofluctuation matrix (TCM) with a window length of 1 TR and sliding windows of 30, 45, and 60 s were utilized, with all windows sliding by a step size of 1 TR. The TCM was constructed by calculating the pointwise product of the z score-normalized BOLD time series for each pair of brain regions:

$$\mathrm{TCM}_{ij}(t) = Z\left(X_i(t)\right) \times Z\left(X_j(t)\right) \quad (2)$$

where $Z\left(X_i(t)\right)$ and $Z\left(X_j(t)\right)$ are the z score normalized BOLD signals for regions i and j at time point t. This calculation results in a dynamic connectivity matrix for each time point. Regions that fluctuated in the same direction presented positive cofluctuation values, whereas opposite fluctuations yielded negative values. Averaging these matrices over time yielded the Pearson correlation coefficient typically used to define FC (Cao et al. 2020). We constructed sliding temporal windows of 10, 15, and 20 TRs, a range that is reportedly able to capture resting-state DFC fluctuations (Preti et al. 2017). This window subsequently slid along the time course with a step of 1 TR (3 s). We then calculated FC in accordance with SFC analysis in each window, resulting in a time series of FC matrices (400 × 400, Fisher z-transformed) for the next analysis.

2.4 | Static and Dynamic SFC Calculations

To calculate region-specific SFC, we developed a multiple linear regression model to predict the FC of node i on the basis of the SC profiles between node i and all other nodes $j \neq i$ (Vázquez-Rodríguez et al. 2019). The model incorporates several predictors, including the Euclidean distance, shortest path length, and communicability. The Euclidean distance was computed between the centroids of the nodes, while the shortest path length referred to the minimal number of edges between two nodes. The communicability C_{ij} between nodes i and j was defined as the weighted sum of all paths and walks between these nodes (Estrada and Hatano 2008). For a weighted adjacency matrix A, communicability was calculated as in Equation (3), where $D = \mathrm{diag}\left(\sum_{k=1}^{N} a_{ik}\right)$ is the diagonal matrix of the generalized node degree (Crofts and Higham 2009). The SC matrix for each individual was standardized, and before the shortest path length was calculated, the structural connection weights were transformed using a negative logarithm (Avena-Koenigsberger et al. 2017).

$$C_{ij} = \left(\exp\left(D^{-1/2}AD^{-1/2}\right)\right)_{ij} \quad (3)$$

For each node i of subject s at time point t, the FC feature was modeled using the linear regression as follows:

$$\mathrm{FC}(s,t,i) = \beta 0 + \beta 1 \times \mathrm{dist}(i) + \beta 2 \times \mathrm{spl}(s,i) + \beta 3 \times \mathrm{cmc}(s,i) + \epsilon \quad (4)$$

where $\mathrm{FC}(s,\mathrm{t},i)$ represents the FC feature of brain region i for subject s at time point t with respect to all other brain regions. This feature was predicted on the basis of the following variables: the Euclidean distance $\mathrm{dist}(i)$, the shortest path length $\mathrm{spl}(s,i)$, and the weighted communicability $\mathrm{cmc}(s,i)$ of region i with the other regions for subject s. The regression coefficients $\beta 0$, $\beta 1$, $\beta 2$, and $\beta 3$ were estimated using ordinary least squares. The strength of the structure–function relationship was quantified using the goodness-of-fit of the regression model, with the coefficient of determination R^2 used as the measure of SFC, as shown in Figure 1.

To calculate static SFC, a unique R^2 value was assigned to each brain region without time, representing the coupling relationship between SC and FC. This value is independent of time and reflects the static SFC.

The dynamic SFC was calculated using the SFC values within each time window for each brain region, thereby forming a time series of dynamic SFC for all brain regions. Then, we established two essential measures to examine the changes in dynamic SFC associated with disease progression: (1) standard deviation (SD), which quantifies the variability of dynamic SFC, is calculated as the standard deviation of the SFC time series for each region. A greater SD indicates greater fluctuations in the dynamic SFC. (2) Recurrence rate (RR), which measures the stability of the dynamic SFC. A greater RR reflects a more frequent recurrence of states, indicating increased stability in dynamic SFC. RR was calculated as the proportion of recurrent states in the time series as in Equation (5), where Θ is the Heaviside function and where ϵ is a threshold parameter.

$$\mathrm{RR} = \frac{1}{N^2}\sum_{i=1}^{N}\sum_{j=1}^{N}\Theta\left(\epsilon - \left|x_i - x_j\right|\right) \quad (5)$$

After static SFC and dynamic SFC were obtained, taking potential batch effects into consideration, we applied Combat harmonization to SFC features using the neuroCombat algorithm to the SFC features across the discovery cohort and the external validation cohort. This algorithm can estimate and eliminate scanner-related technical differences while preserving true biological signals, enhancing data comparability across different scanners and improving the accuracy and generalizability of the research findings (Fortin et al. 2017, 2018).

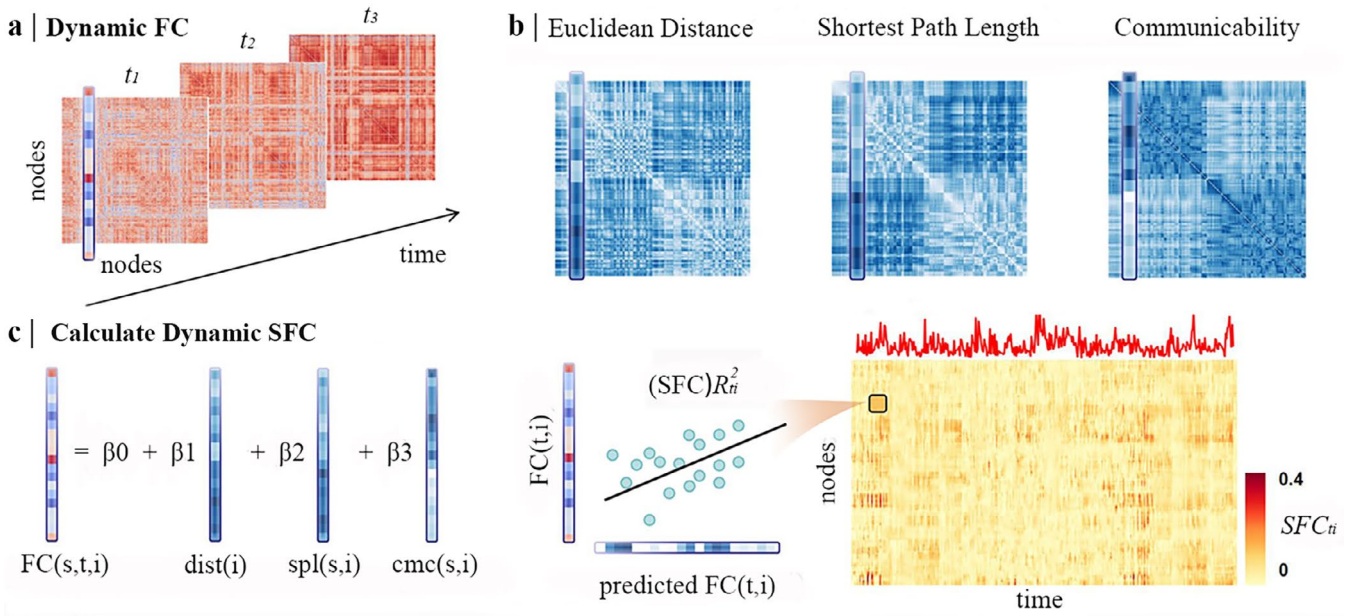

FIGURE 1 | Dynamic SFC Calculation. (a) Calculation of dynamic FC; (b) multiple computational models of cortical communication used in the regression model; (c) calculation of dynamic SFC. s represents the subject s, t represents the time point t, i represents the brain region i, dist(i) represents the Euclidean distance between brain region i and other brain regions, spl(s, i) represents the shortest path length between brain region i and other brain regions for subject s, cmc(s, i) represents the communicability between brain region i and other brain regions for subject s, and R_{ti}^2 represents the SFC value of brain region i at time point t.

2.5 | Overlap Between SFC Features and Braak Stages

To investigate whether SFC features can effectively reflect the pathological changes caused by tau protein accumulation in AD patients, we analyzed the overlap between brain regions exhibiting significant SFC feature changes and those defined by the Braak stage template.

We performed an analysis of variance (ANOVA) followed by multiple comparison correction and analyzed the overlap between SFC feature brain regions with significant group differences and the brain regions defined by the Braak stage template. Overlap was identified when 60% of the voxels of the SFC feature brain regions coincided with the voxels of the Braak stage regions.

2.6 | Feature Selection and Classification

Next, we used the SFC features combined with ML methods to perform stage-specific classification of AD patients. To improve the classification performance of the model and reduce overfitting, we first used ElasticNet for feature selection, followed by ML classifiers for classification. The ElasticNet objective function is as follows:

$$\min_{\beta}\left\{\frac{1}{2n}\sum_{i=1}^{n}\left(y_i - X_i\beta\right)^2 + \lambda_1\sum_{j=1}^{p}\left|\beta_j\right| + \lambda_2\sum_{j=1}^{p}\beta_j^2\right\} \quad (6)$$

This objective function combines the L1 regularization term $\lambda_1\sum_{j=1}^{p}\left|\beta_j\right|$, which encourages sparsity, and the L2 regularization term $\lambda_2\sum_{j=1}^{p}\beta_j^2$, which penalizes large coefficients, allowing ElasticNet to select important features while maintaining model robustness.

The specific steps are as follows: First, ANOVA with multiple comparison correction was used to identify features with significant differences among the HC, MCI, and AD groups. Then, post hoc pairwise t tests (HC vs. MCI, MCI vs. AD) were conducted to further refine these features and ensure their statistical significance. Next, ElasticNet was used to perform feature selection on the filtered features. Finally, a range of linear and nonlinear classifiers were employed for classification.

Before classification, we adjusted the SFC features by removing the effects of covariates such as age, sex, and years of education. To account for these covariates, we applied a linear regression model. The adjusted SFC feature, denoted as SFC′, was calculated as the residual from this regression model in Equation (7):

$$\mathrm{SFC}' = \mathrm{SFC} - \beta_1 \times \mathrm{age} - \beta_2 \times \mathrm{sex} - \beta_3 \times \mathrm{education} \quad (7)$$

where SFC represents the raw SFC feature values, and β_1, β_2, and β_3 are the regression coefficients corresponding to age, sex, and education, respectively.

The classifiers used included k-nearest neighbors (K-NN), GNB, random forest (RF), support vector machine (SVM), and logistic regression with and without sparse regularization (Dadi et al. 2019), and convolutional neural network (CNN). A grid search was used to optimize the parameters of the K-NN, GNB, RF, SVM, and logistic regression, while the CNN hyperparameters were adjusted through systematic exploration on the basis of the dataset characteristics to enhance model performance. The

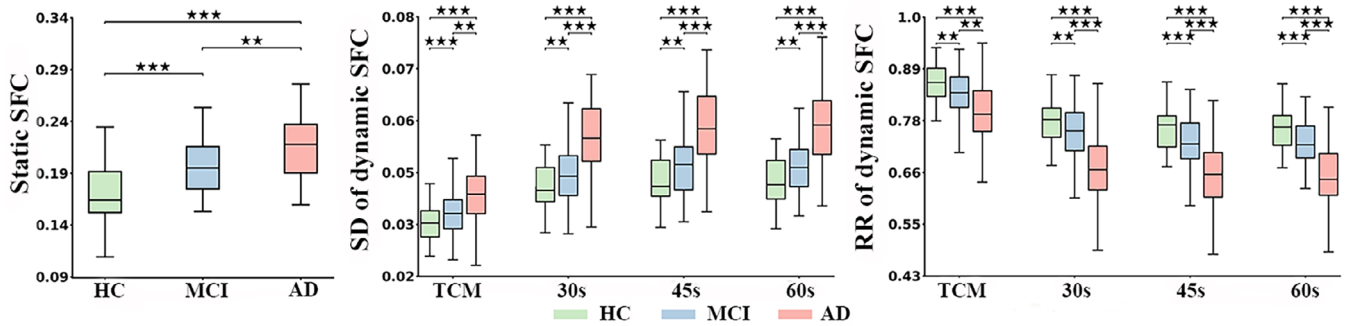

FIGURE 2 | Whole-brain static and dynamic SFC results across HC, MCI, and AD groups. The whole-brain SFC values for the HC, MCI, and AD groups are shown, with different colors representing each group, and significant differences are marked with stars (★★★$p < 0.001$, ★★$p < 0.01$, and ★$p < 0.05$). The *t*-test was used for statistical analysis for data with a normal distribution; otherwise, the Mann–Whitney *U* test was applied, with Bonferroni post hoc correction for significance. TCM represents dynamic SFC with a 1 TR time window, and 30, 45, and 60 s indicate dynamic SFC at respective time window lengths.

models were trained on the discovery dataset and subsequently applied to the external validation set.

2.7 | Analysis of Correlations With Physiological Biomarkers of AD

To explore the potential of SFC features in reflecting the brain's early regulatory response to pathological damage in AD and their possible clinical application value, we examined their correlation with early diagnostic biomarkers of the disease.

We investigated the physiological biomarkers TAU/Aβ42, PTAU/Aβ42, and Aβ42/Aβ40, which are core biomarkers belonging to the initial-stage biomarker category, and were released by NIA-AA in 2024. These biomarkers were all collected from the cerebrospinal fluid samples of the subjects. The NIA-AA 2024 revised criteria affirm that these biomarkers reflect the pathological processes involved in the initial stage of AD, and that they can serve as a reliable basis for the early diagnosis of AD. Using these physiological biomarkers, we conducted partial correlation analyses to assess the relationships between SFC features and these biomarkers. Specifically, Pearson correlation analyses were performed between the mean values of each feature and the biomarkers, controlling for covariates such as age, sex, and years of education to ensure accurate correlation measurements.

Additionally, considering the importance of cognitive function in AD, we further explored the correlation between SFC features and cognitive performance. This allowed us to investigate how SFC features are related to cognitive decline in the context of AD progression. We used averaging of SFC features to enhance data stability and emphasize the most significant patterns, helping to reduce variability and highlighting the core relationships relevant to biomarkers and cognitive performance.

2.8 | Statistical Analysis

All the statistical analyses were conducted using Python, and the demographic data were analyzed via one-way ANOVA and chi-square tests. Pairwise comparisons of whole-brain SFC values and SFC features used for classification were conducted using pairwise tests, with Bonferroni correction applied for whole-brain SFC values. For regional SFC values, one-way ANOVA was first performed to identify regions with significant differences, followed by pairwise tests with FDR correction. These analyses were conducted utilizing the SciPy, Statsmodels, and Scikit-learn libraries. Before pairwise tests were performed, normality checks were conducted. For normally distributed data, *t*-tests were applied: independent t tests for equal variance and Welch's t tests for unequal variance. For nonnormally distributed data, the Mann–Whitney *U* test was used. Accuracy (ACC), specificity (SPC), and sensitivity (SEN) estimates were calculated from the receiver operating characteristic (ROC) curve according to the cutoff value that maximizes the Youden index (sensitivity + specificity − 1). The area under the curve (AUC) was used as the metric for comparing the performance of all the models.

3 | Results

3.1 | Whole-Brain SFC

To explore the changes in SFC with the progression of AD, we first compared the whole-brain static and dynamic SFC results across the HC, MCI, and AD groups. Dynamic SFC was analyzed over four different durations, with the SD and RR used to quantify its variability and stability. As shown in Figure 2, whole-brain static SFC gradually increased with disease progression. The static SFC value for HCs ranged from 0.10 to 0.24, that for the MCI group ranged from 0.15 to 0.25, and that for the AD group ranged from 0.16 to 0.27. From HC to MCI, static SFC significantly increased, with greater significance than that observed from MCI to AD. The SD of dynamic SFC also showed an increasing trend across all time windows. Except for TCM, the increase in SD across all time window lengths was significantly greater in the HC–MCI stage than in the MCI–AD stage. In contrast, the RR of dynamic SFC gradually decreases with disease progression. Except for the 30 s time window, where the significance of the decrease in RR was slightly greater in the HC–MCI stage than in the MCI–AD stage, the changes in other time window lengths were not significantly different between the two stages. These results indicate that as AD progresses,

static SFC gradually increases, and dynamic SFC variability increases but stability decreases. Specific p-values for these results are provided in Table S1.

Additionally, we presented the overlapping regions between the brain regions characterized by SFC features with significant differences across the three groups and the brain regions defined by the Braak stage, demonstrating the correspondence between these SFC features and Braak pathological stages (Figure 3, Table 2).

We found that the feature regions for both static and dynamic SFC significantly overlapped with the Braak stage regions. The static SFC feature regions overlapped with one region of Braak stage III, three regions of stage IV, two regions of stage V, and three regions of stage VI. For dynamic SFC, the brain regions where SD and RR showed significant group differences across all time windows had the most overlap with Braak stage V. Except for the RR feature at the 45 and 60 s time windows, no overlap was observed with Braak stage III brain regions. Except for the 30 s time window, the overlap between the dynamic SFC features and Braak stage IV features was less than that between the static SFC features and the other time window lengths. These results indicate that with the progression of AD, static and dynamic SFC feature regions gradually overlap with different brain regions defined by Braak stages, reflecting the relationships between these features and the pathological stages of AD. Notably, the lack of overlap with Braak stages I and II may be because MCI and AD patients are mainly at Braak stages III and above (Biel et al. 2021).

3.2 | Combination of SFC and ML in AD Classification

To evaluate the classification performance of different classifiers and SFC features in the HC–MCI and MCI–AD stages, we compared the binary classification performance using SFC, SC, and FC features across both stages. The models were trained on the ADNI dataset and validated on an in-house dataset. Initially, ANOVA was performed on regional SFC values to identify regions with significant differences, followed by pairwise comparisons with FDR correction. The final feature selection was carried out using the ElasticNet method. The results are presented in Figure 4 and Figure 5.

As shown in Figure 4, the GNB classifier consistently outperformed all the other classifiers in both the HC–MCI and MCI–AD classifications. In the HC–MCI stage, in terms of classification performance, the static SFC consistently outperformed the other features across all classifiers, whereas in the MCI–AD stage, the SD feature of dynamic SFC generally

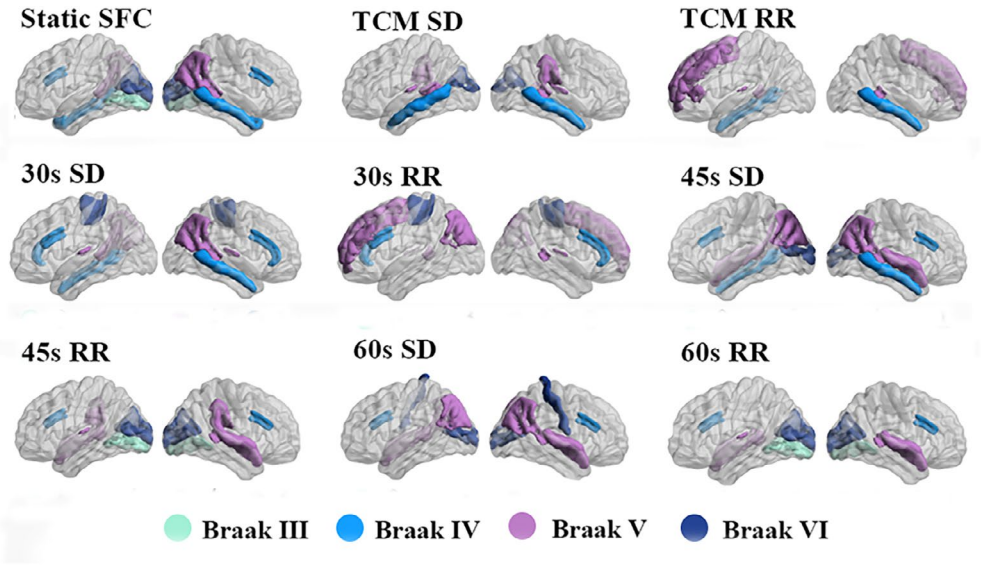

FIGURE 3 | Overlapping brain regions between SFC features and Braak stage regions. The overlap between static and dynamic feature regions and the Braak stage regions is shown, with different colors representing Braak stages III–VI, as indicated in the legend.

TABLE 2 | Overlapping brain regions.

Braak	Static SFC	TCM SD	TCM RR	30 s SD	30 s RR	45 s SD	45 s RR	60 s SD	60 s RR
III	1	0	0	0	0	0	1	0	1
IV	3	2	1	4	3	2	1	1	1
V	2	5	5	4	5	5	4	5	3
VI	3	1	0	1	1	1	3	4	4

Note: The numbers in the table represent the number of overlapping brain regions for each Braak stage. The SFC feature regions are defined as those showing significant group differences in a one-way ANOVA with FDR post hoc correction.

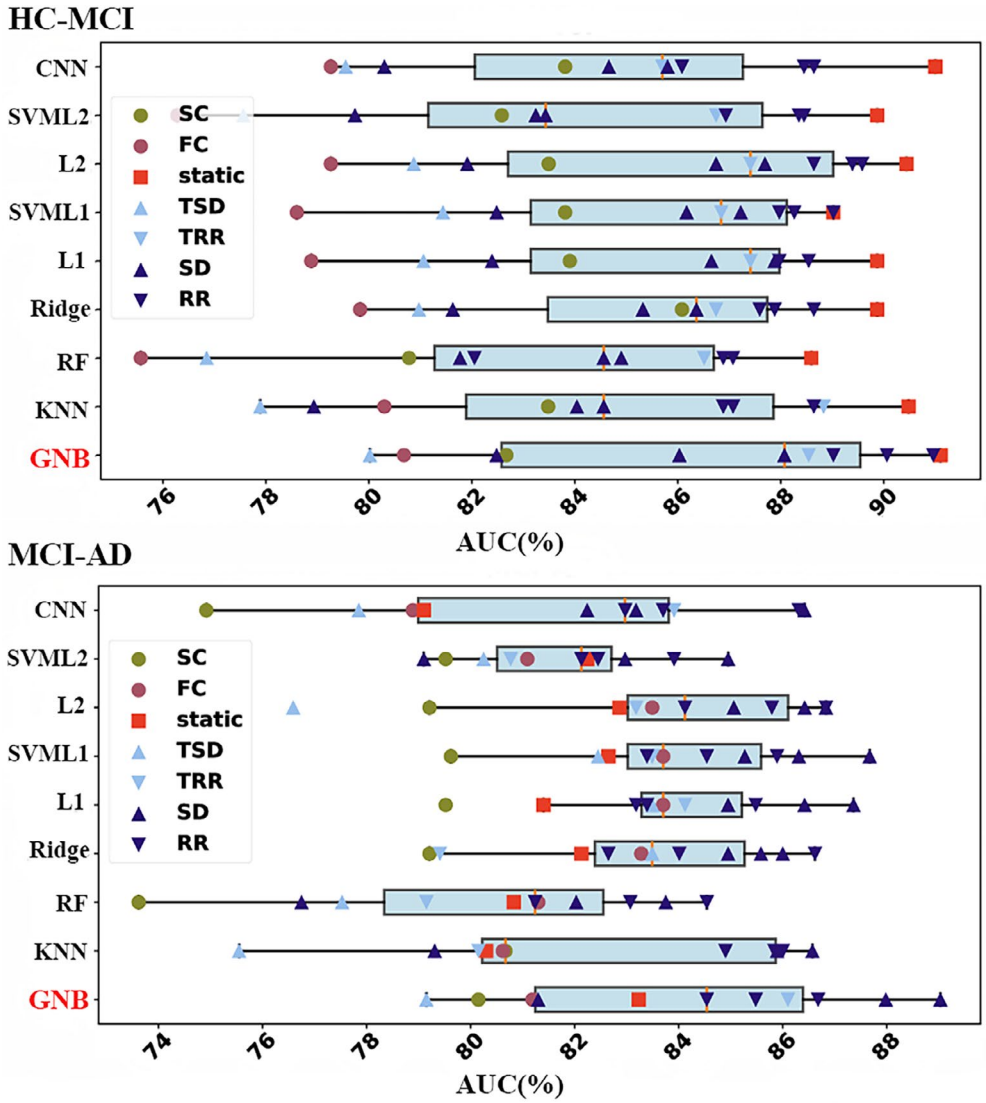

FIGURE 4 | Performance of different classifiers represented by AUC values. Top image: Classification performance for the HC vs. MCI stage; Bottom image: Classification performance for the MCI versus AD stage. The horizontal axis represents area under the curve (AUC) values, and the vertical axis lists the different classification algorithms. The features used include static SFC, dynamic SFC metrics (with time windows of 30, 45, and 60 s: Features SD, RR, and the TCM SD, RR features: TSD, TRR), communicability and the shortest path between brain region nodes (SC), functional connectivity (FC). Different features are distinguished by the colors and symbols shown in the legend.

outperformed the other features across all classifiers. Notably, except for the SD and RR features of the TCM, both the dynamic and static SFC features generally outperformed the SC or FC features alone.

We also determined the ranking of classification performance (measured by AUC) for all features using the GNB classifier in both the HC–MCI and MCI–AD stages, along with the ROC curves for the five features with the best classification performance in each stage (Figure 5). Among the SFC features, static SFC exhibited the best performance in the HC–MCI stage, with an ACC of 87.69%, SEN of 90.91%, SPC of 84.38%, and AUC of 91.10%. In contrast, in the MCI–AD stage, the SD feature of dynamic SFC (with a 60-s time window) exhibited the best performance, with an ACC of 83.87%, SEN of 82.76%, SPC of 90.01%, and AUC of 89.03%. These results indicate that the GNB classifier outperformed all other classifiers in both the HC–MCI and MCI–AD stages, with SFC features consistently outperforming single features in all stages. Specifically, static SFC demonstrated the best classification performance in the HC–MCI stage, whereas the SD feature of dynamic SFC (with a 60-s time window) demonstrated the best performance in the MCI–AD stage. These results indicate that the classification performance of SFC features outperforms that of individual SC and FC features and that the combination of ElasticNet and GNB yields the best classification performance for SFC features.

3.3 | Brain Network of SFC Features in AD

We also analyzed the changes in static and dynamic SFC features with the best classification performance across AD progression and their distributions across specific brain regions, as shown in Figures 6 and 7. Static SFC features, derived from the HC–MCI stage binary classification, include 18 regions, which are primarily concentrated in the sensorimotor network (SMN),

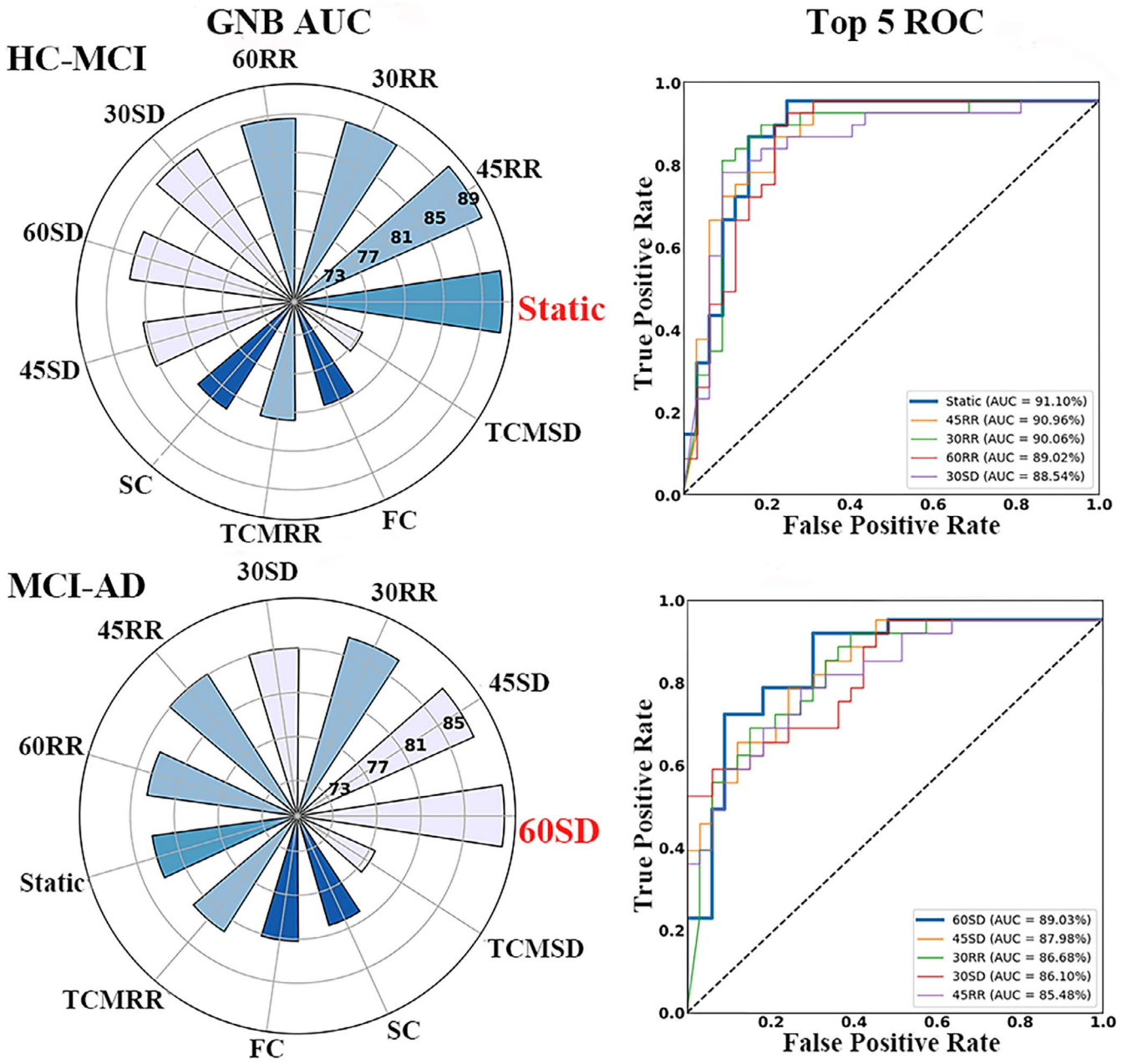

FIGURE 5 | Performance of classification features using GNB. Top image: Ranking of AUC values for all features classified using the GNB classifier in the HC–MCI stage, along with the ROC curves for the top five features with the best classification performance. Bottom image: Ranking of AUC values for all features classified using the GNB classifier in the MCI–AD stage, along with the ROC curves for the top five features with the best classification performance. Here, 30, 45, and 60 correspond to different time window lengths, and the gridlines represent the AUC values.

dorsal attention network (DAN), and default mode network (DMN). Dynamic SFC features, represented by the SD of dynamic SFC within a 60-s time window from the MCI–AD stage classification, include 14 regions distributed across all functional networks. The specific brain regions corresponding to the region numbers are provided in the Table S2.

Static SFC features exhibited significant changes during the HC–MCI stage but tended to stabilize in the MCI–AD stage (Figure 6). In contrast, dynamic SFC features showed minimal significant changes in the HC–MCI stage but became significantly variable in the MCI–AD stage. Additionally, we observed that both static and dynamic SFC features included regions within the right middle cingulum (Cingulum_mid_R), as defined by the AAL atlas, as illustrated in Figure 7. These results indicate that static and dynamic SFC features exhibit different patterns of change during AD progression, and both show significant changes in Cingulum_mid_R.

3.4 | Correlation of SFC With Early AD Biomarkers

To explore the relationships between SFC features and physiological biomarkers, we calculated the correlations between the best-performing SFC classification features and TAU/Aβ42,

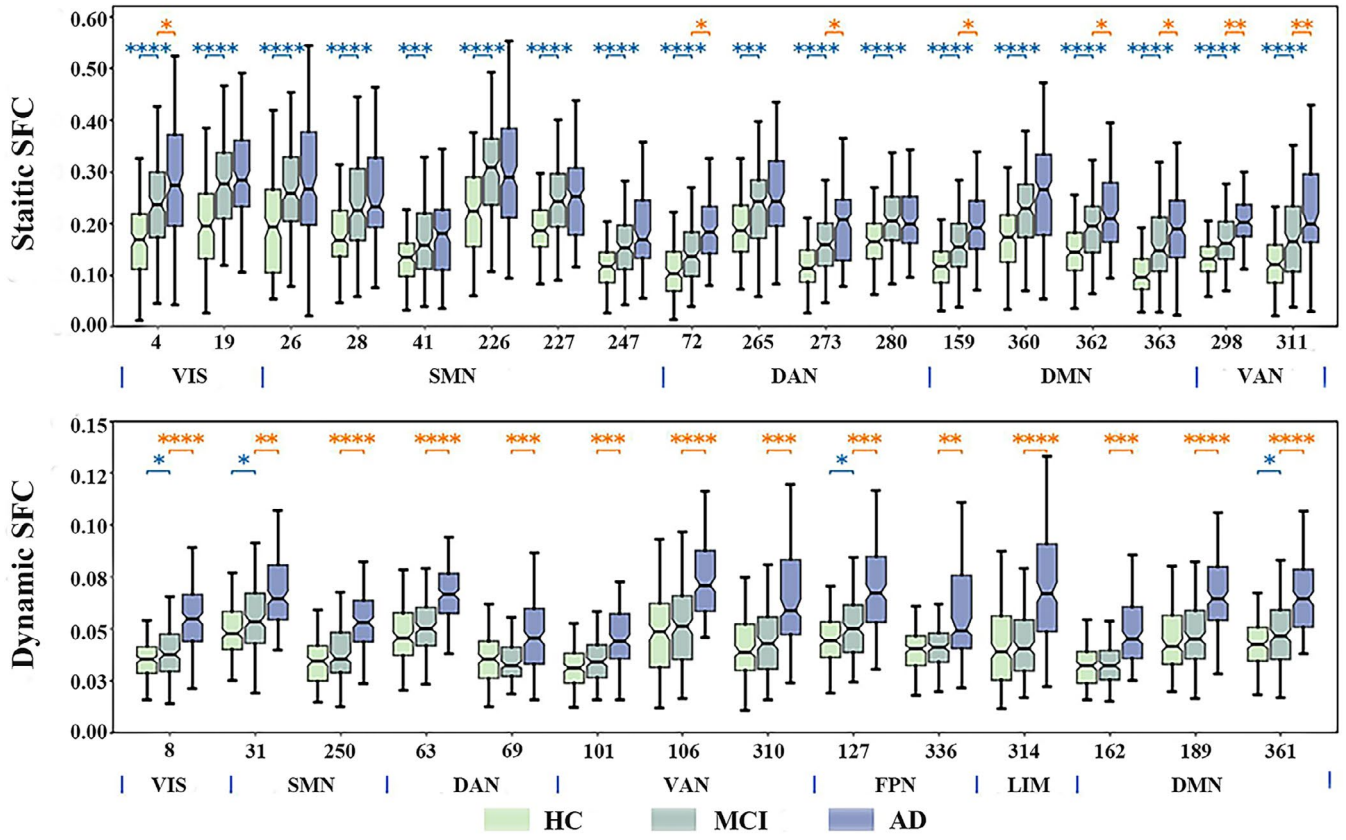

FIGURE 6 | Brain region distributions and progression of the best SFC features. The *x*-axis represents brain region numbers and their corresponding functional networks. The *y*-axis represents the static SFC in the upper panel and the SD values of dynamic SFC within a 60-s time window in the lower panel. Blue asterisks indicate significant differences between the HC and MCI groups, and orange asterisks indicate significant differences between the MCI and AD groups (*$p<0.05$, **$p<0.01$, ***$p<0.001$, and ****$p<1e{-}4$). The *t*-test was used for normally distributed data; otherwise, the Mann–Whitney U test was applied, with Bonferroni post hoc correction for significance. DAN, dorsal attention network; DMN, default mode network; FPN, frontoparietal network; LIM, limbic network; SMN, sensorimotor network; VAN, ventral attention network; VIS, visual network.

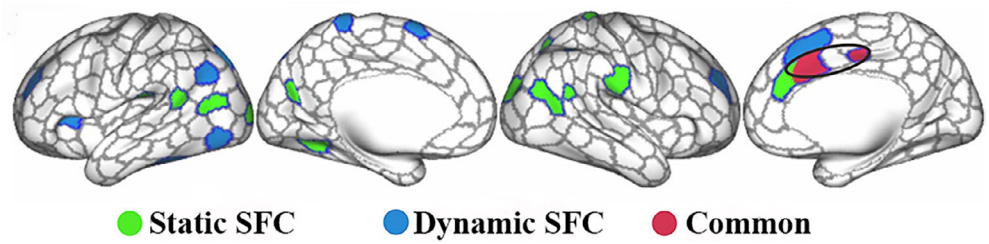

FIGURE 7 | Common regions in AAL with feature distribution: Green for static SFC features, blue for dynamic SFC features. Red regions within black circles indicate overlap, with the left showing static and the right showing dynamic SFC features in the right middle cingulum.

PTAU/Aβ42, and Aβ42/Aβ40, as well as cognitive scales (MMSE and MOCA), as shown in Figure 8.

After controlling for covariates such as age, sex, and years of education, we found that both static and dynamic SFC features were significantly correlated with early AD biomarkers and cognitive performance. Static classification features were significantly positively correlated with TAU/Aβ42 ($r=0.430$, $p<0.001$) and PTAU/Aβ42 ($r=0.429$, $p<0.001$) and significantly negatively correlated with Aβ42/Aβ40 ($r=-0.356$, $p<0.001$). Additionally, static features showed strong negative correlations with MMSE ($r=-0.533$, $p<0.001$) and MOCA ($r=-0.601$, $p<0.001$) scores, indicating that greater SFC coupling is associated with worse cognitive performance. Dynamic classification features were significantly positively correlated with TAU/Aβ42 ($r=0.289$, $p<0.001$) and PTAU/Aβ42 ($r=0.257$, $p=0.001$) and significantly negatively correlated with Aβ42/Aβ40 ($r=-0.271$, $p=0.003$).

Furthermore, dynamic features were also significantly negatively correlated with MMSE ($r=-0.522$, $p<0.001$) scores and MOCA ($r=-0.533$, $p<0.001$), reinforcing the association between SFC features and cognitive decline. These results suggest that both static and dynamic SFC features are significantly correlated with early AD biomarkers and cognitive impairment, with static features showing slightly stronger correlations than dynamic features.

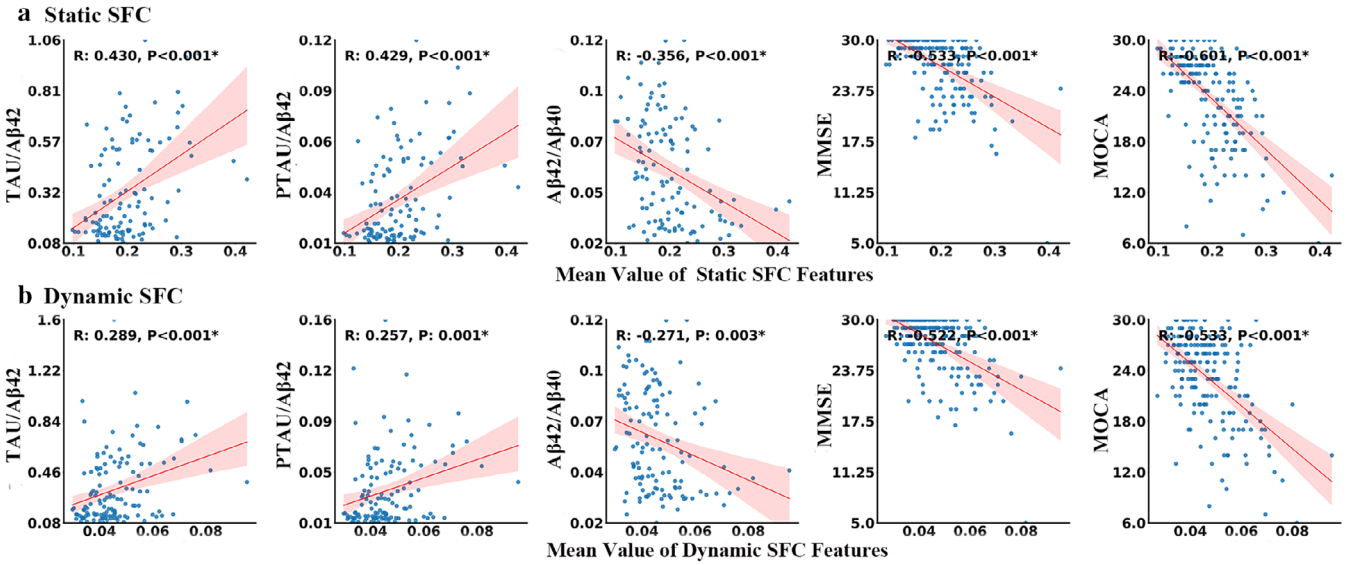

FIGURE 8 | The figure illustrates the correlation between coupling features and early AD biomarkers, as well as cognitive scales. (a) Static SFC classification features; (b) dynamic SFC features representing the 60-s standard deviation. From left to right, the three biomarkers and two cognitive scales are TAU/Aβ42, PTAU/Aβ42, Aβ42/Aβ40, MMSE, and MOCA. * indicates statistical significance. The horizontal axis represents the average value calculated from the SFC feature brain regions that contributed most significantly to the classification task.

4 | Discussion

Our findings indicate that the increase in static SFC is closely associated with AD progression, suggesting that the brain increasingly relies on existing structural connections to maintain function in AD. This finding is consistent with those of previous studies (Cao et al. 2020; Dai et al. 2019), which also highlighted the increased static SFC as AD progresses. This reliance may result from the loss of neurons and synapses in AD, gradually reducing the ability of the brain to establish new functional pathways or compensatory connections (Terry et al. 1991). This process is reflected in the progressive weakening and disruption of the SC and FC. As AD progresses, dynamic SFC shows greater variability and less stability, indicating a reduced capacity of SC to maintain stable dynamic connectivity. Gu et al. reported that decreased regional temporal variability was significantly correlated with the cognitive performance of AD patients (Gu et al. 2020). Additionally, Núñez et al. reported that AD patients exhibited more unstable dynamic brain activity during the resting state (Núñez et al. 2021). These findings suggest that as SC deteriorates, its support for dynamic FC weakens, limiting the adaptability of the brain under pathological stress.

The Braak staging system, which is based on the accumulation and spread of tau protein during AD progression, outlines the key affected brain regions. AD progression can be divided into six stages, beginning with tau pathology in the entorhinal cortex and hippocampus and later spreading to other areas of the cerebral cortex (Braak and Braak 1991). Our study revealed that brain regions exhibiting significant intergroup differences in SFC overlapped with those defined in Braak stages III–VI. This overlap may be related to the accumulation of the tau protein, which causes synaptic damage, thereby weakening FC and ultimately affecting the SFC (Li et al. 2018; Wu et al. 2021). Our findings suggest that these SFC abnormalities not only statistically coincide but also reflect the potential value of SFC features in AD.

In the HC–MCI stage, SC remains largely preserved, enabling the brain to maintain functional stability through the support of SC in functional processes (Filippi et al. 2020). This early-stage compensation mechanism allows static SFC to capture the increased reliance of the function on the structure. This increase in static SFC serves as a reliable feature for distinguishing HCs from MCI patients, highlighting the functional stability maintained by structural integrity during the early stage of AD. In the MCI–AD stage, SC undergoes widespread damage, and the stability of dynamic FC significantly decreases (Qing et al. 2021). Dynamic SFC is capable of capturing transient fluctuations in brain activity that traditional static SFC cannot detect; these fluctuations reflect the dynamic characteristics of SFC that continuously adjust as the disease progresses. The increase in dynamic SFC variability reflects the instability in SC capacity to regulate dynamic brain activity, indicating a gradual disruption of functional dynamic homeostasis during AD progression. The high sensitivity of dynamic SFC makes it a key tool for studying the adaptive mechanisms of the brain in the MCI–AD stage while providing new insights into the pathological progression of AD.

By integrating ElasticNet and GNB, the SFC features achieved superior classification performance in distinguishing different stages of AD, significantly outperforming the effectiveness of single FC or SC features. In the external validation set, static SFC features reached an AUC of 91.10% for HC versus MCI, whereas dynamic SFC features attained an AUC of 89.03% for MCI versus AD. SFC combines structural and functional patterns to provide a more comprehensive reflection of the brain's state, offering a more representative evaluation of cognitive ability and disease progression than SC or FC alone does (Fotiadis et al. 2024). However, SFC shows relatively poor performance in

terms of TCM time window features, possibly because the short TCM time window limits the capture of neural complexity and coupling interactions, mingles neural fluctuations with noise, and increases data variability. The combination of ElasticNet and GNB outperformed classifiers such as KNN, SVM, RF, and logistic regression due to their complementary strengths. ElasticNet effectively captures the most discriminative SFC features through feature selection and regularization, minimizing overfitting and removing irrelevant information (Zou and Hastie 2005). GNB, which assumes feature independence, aligns seamlessly with the features selected by ElasticNet, enabling efficient and accurate classification (Wickramasinghe and Kalutarage 2021). In contrast, KNN relies on distance metrics, making it sensitive to irrelevant features in high-dimensional spaces, which reduces classification accuracy (Guo et al. 2003). SVMs often struggle with small datasets due to overfitting and require extensive hyperparameter tuning (Wien et al. 2007). RF faces challenges with inconsistent feature importance rankings and high computational demands, affecting classification consistency (Parmar et al. 2019). Logistic regression, especially without sparse regularization, fails to capture nonlinear relationships, limiting its generalizability in complex feature spaces (Dreiseitl and Ohno-Machado 2002). CNN may be restricted by the absence of a clear spatial structure in data features and small dataset sizes, which undermines its classification performance (Li et al. 2022). The synergy between ElasticNet's targeted feature selection and GNB's efficient classification process provides a streamlined and highly effective approach, offering superior classification performance and generalization in SFC-based tasks.

The static SFC features used for classification in the HC–MCI stage are primarily concentrated in the SMN, DAN, and DMN. AD patients experience progressive declines in sensorimotor abilities, attention, and self-referential processing, which correspond to disruptions in these networks (Kim 2012). The DMN is widely acknowledged as a central functional network in AD. Studies have shown that key nodes within the DMN, such as Right_DefaultA_PCC_1 in the posterior cingulate cortex, undergo significant functional and structural disruptions in MCI, making them among the earliest affected regions (Lee et al. 2020).

The dynamic SFC features used for classification in the MCI–AD stage are widely distributed, which may be attributed to the extensive myelin loss that occurs during the progression of AD (Maitre et al. 2023; Nasrabady et al. 2018). Myelin, an insulating layer around nerve fibers, is essential for the normal transmission of signals between neurons and the synchronization of neuronal activities. A reduction in myelin impairs the conduction velocity of nerve impulses, disrupts neuronal firing patterns, and weakens the correlation between brain structure and function, which over time may exacerbate the deviation of this correlation from its mean value, ultimately increasing the variability of dynamic SFC (Fotiadis et al. 2023; Wang et al. 2020). The dynamic SFC features are most numerous in the regions in the DMN and VAN. The VAN is closely related to AD and plays a key role in attention allocation and response to salient stimuli (Zhang et al. 2015). Research has shown that AD patients exhibit lower temporal stability in VAN regions, which is significantly associated with cognitive decline, suggesting that VAN instability may exacerbate cognitive deficits in AD patients (Chumin et al. 2021). Additionally, both static and dynamic SFC classification features involve the Cingulum_mid_R region, a core hub for attention, emotional regulation, and memory integration. Multiple studies have reported significant changes in this region during AD progression (Bozzali et al. 2012; Bubb et al. 2018). These findings suggest that SFC features are sensitive to changes in key brain regions, underscoring the importance of SFC in understanding AD progression.

According to the 2024 revised criteria from the National Institute on Aging and Alzheimer's Association, TAU/Aβ42, PTAU/Aβ42, and Aβ42/Aβ40 are important physiological biomarkers for AD. These ratios reflect changes in cerebrospinal fluid tau and β-amyloid levels, indicating early AD pathology. The abnormal accumulation of tau protein, the accumulation of phosphorylated tau, and the reduction in Aβ42 lead to increases in the TAU/Aβ42 and PTAU/Aβ42 ratios and a decrease in the Aβ42/Aβ40 ratio. Hyperphosphorylated tau accumulates in Alzheimer's disease, forming neurofibrillary tangles. Moreover, the reduction in Aβ42 signals the deposition of amyloid plaques and is accompanied by neuroinflammation, leading to neuronal damage and synaptic dysfunction. These pathological changes ultimately result in neurodegenerative alterations, which often appear in the early stages of AD (Jack et al. 2024). Our study revealed that the SFC features were significantly positively correlated with the TAU/Aβ42 and PTAU/Aβ42 ratios and significantly negatively correlated with the Aβ42/Aβ40 ratio. Additionally, they were negatively correlated with cognitive performance, as reflected by the MMSE and MOCA scores. These findings suggest that, in the early stages, the brain may adjust the SFC to mitigate pathological damage, while also capturing early cognitive decline, highlighting the potential value of SFC features in the early diagnosis of AD.

This study has several limitations. First, it did not distinguish between MCI subtypes, which may affect the understanding of their distinct characteristics and progression. Future studies should explore these differences for a more comprehensive analysis. Second, ML-based methods require large and diverse datasets to extract features efficiently and ensure robust performance. However, the amount of data used in this study was small, mainly consisting of Caucasian participants (ADNI dataset) and Asian participants (in-house dataset), which may limit the model's generalizability. Future research should include more diverse datasets and more complex models to improve robustness and applicability across different populations. Third, this study was a cross-sectional study. To fully understand the interaction between structural and functional abnormalities in AD, further longitudinal studies are necessary.

5 | Conclusion

This study systematically examined the differences in static and dynamic SFC features across AD progression, highlighting their potential in neurological diseases. These findings indicate that static SFC significantly increases, whereas dynamic SFC shows greater fluctuations and reduced stability as AD progresses. Notably, the regions of interest with significant

SFC differences overlap with Braak staging regions, underscoring the relevance of these features to AD pathology. By integrating ElasticNet with GNB, we achieved high classification performance in distinguishing the HC–MCI and MCI–AD stages. Additionally, both static and dynamic SFC classification features were significantly correlated with physiological and cognitive performance, especially in the Cingulum_mid_R region. These features, as sensitive markers for early AD, offer opportunities for timely intervention and personalized treatments aimed at slowing disease progression and improving quality of life. Overall, our findings underscore the importance of combining dynamic and static SFC in understanding AD mechanisms and the potential of this method for the early detection of AD.

Author Contributions

Han Wu: conceptualization, investigation, data curation and analysis, manuscript writing – original draft, visualization. **Yinping Lu:** conceptualization, methodology, data curation, validation. **Jinglong Wu:** conceptualization, supervision, funding acquisition. **Ying Liu:** conceptualization, supervision. **Zhilin Zhang:** conceptualization, validation, methodology, visualization, project administration, manuscript writing – review and editing, funding acquisition. **Luyao Wang:** conceptualization, methodology, validation, writing – review and editing, supervision.

Acknowledgments

This work was supported by GuangDong Basic and Applied Basic Research Foundation (2023A1515012929); Science and Technology Planning Project of Guangdong Province, China (2023A0505050162).

Conflicts of Interest

The authors declare no conflicts of interest.

Data Availability Statement

The data that support the findings of this study are available on request from the corresponding author. The data are not publicly available due to privacy or ethical restrictions.

References

Anand, M. V., B. KiranBala, S. R. Srividhya, C. K, M. Younus, and M. H. Rahman. 2022. "Gaussian Naïve Bayes Algorithm: A Reliable Technique Involved in the Assortment of the Segregation in Cancer." *Mobile Information Systems* 2022: 2436946. https://doi.org/10.1155/2022/2436946.

Avena-Koenigsberger, A., B. Mišić, R. X. D. Hawkins, et al. 2017. "Path Ensembles and a Tradeoff Between Communication Efficiency and Resilience in the Human Connectome." *Brain Structure & Function* 222: 603–618.

Batista-García-Ramó, K., and C. I. Fernández-Verdecia. 2018. "What We Know About the Brain Structure–Function Relationship." *Behavioral Science* 8: 39.

Baum, G. L., Z. Cui, D. R. Roalf, et al. 2020. "Development of Structure–Function Coupling in Human Brain Networks During Youth." *Proceedings of the National Academy of Sciences* 117: 771–778.

Biel, D., M. Brendel, A. Rubinski, et al. 2021. "Tau-PET and In Vivo Braak-Staging as Prognostic Markers of Future Cognitive Decline in Cognitively Normal to Demented Individuals." *Alzheimer's Research & Therapy* 13: 137.

Bozzali, M., G. Giulietti, B. Basile, et al. 2012. "Damage to the Cingulum Contributes to Alzheimer's Disease Pathophysiology by Deafferentation Mechanism." *Human Brain Mapping* 33: 1295–1308.

Braak, H., and E. Braak. 1991. "Neuropathological Stageing of Alzheimer-Related Changes." *Acta Neuropathologica* 82: 239–259.

Bubb, E. J., C. Metzler-Baddeley, and J. P. Aggleton. 2018. "The Cingulum Bundle: Anatomy, Function, and Dysfunction." *Neuroscience & Biobehavioral Reviews* 92: 104–127.

Cao, R., X. Wang, Y. Gao, et al. 2020. "Abnormal Anatomical Rich-Club Organization and Structural–Functional Coupling in Mild Cognitive Impairment and Alzheimer's Disease." *Frontiers in Neurology* 11: 53. https://doi.org/10.3389/fneur.2020.00053.

Cha, J., H. J. Jo, H. J. Kim, et al. 2013. "Functional Alteration Patterns of Default Mode Networks: Comparisons of Normal Aging, Amnestic Mild Cognitive Impairment and Alzheimer's Disease." *European Journal of Neuroscience* 37: 1916–1924.

Chen, Y., Y. Wang, Z. Song, Y. Fan, T. Gao, and X. Tang. 2023. "Abnormal White Matter Changes in Alzheimer's Disease Based on Diffusion Tensor Imaging: A Systematic Review." *Ageing Research Reviews* 87: 101911.

Chumin, E. J., S. L. Risacher, J. D. West, et al. 2021. "Temporal Stability of the Ventral Attention Network and General Cognition Along the Alzheimer's Disease Spectrum." *NeuroImage: Clinical* 31: 102726.

Collin, G., L. H. Scholtens, R. S. Kahn, M. H. J. Hillegers, and M. P. van den Heuvel. 2017. "Affected Anatomical Rich Club and Structural–Functional Coupling in Young Offspring of Schizophrenia and Bipolar Disorder Patients." *Biological Psychiatry* 82: 746–755.

Crofts, J. J., and D. J. Higham. 2009. "A Weighted Communicability Measure Applied to Complex Brain Networks." *Journal of the Royal Society Interface* 6: 411–414.

Cui, Z., S. Zhong, P. Xu, G. Gong, and Y. He. 2013. "PANDA: A Pipeline Toolbox for Analyzing Brain Diffusion Images." *Frontiers in Human Neuroscience* 7: 42. https://doi.org/10.3389/fnhum.2013.00042.

Dadi, K., M. Rahim, A. Abraham, et al. 2019. "Benchmarking Functional Connectome-Based Predictive Models for Resting-State fMRI." *NeuroImage* 192: 115–134.

Dai, Z., Q. Lin, T. Li, et al. 2019. "Disrupted Structural and Functional Brain Networks in Alzheimer's Disease." *Neurobiology of Aging* 75: 71–82.

Demirtaş, M., C. Falcon, A. Tucholka, J. D. Gispert, J. L. Molinuevo, and G. Deco. 2017. "A Whole-Brain Computational Modeling Approach to Explain the Alterations in Resting-State Functional Connectivity During Progression of Alzheimer's Disease." *NeuroImage: Clinical* 16: 343–354.

Dreiseitl, S., and L. Ohno-Machado. 2002. "Logistic Regression and Artificial Neural Network Classification Models: A Methodology Review." *Journal of Biomedical Informatics* 35: 352–359.

Esteban, O., C. J. Markiewicz, R. W. Blair, et al. 2019. "fMRIPrep: A Robust Preprocessing Pipeline for Functional MRI." *Nature Methods* 16: 111–116.

Estrada, E., and N. Hatano. 2008. "Communicability in Complex Networks." *Physical Review E* 77: 036111.

Filippi, M., S. Basaia, E. Canu, et al. 2020. "Changes in Functional and Structural Brain Connectome Along the Alzheimer's Disease Continuum." *Molecular Psychiatry* 25: 230–239.

Fortin, J.-P., N. Cullen, Y. I. Sheline, et al. 2018. "Harmonization of Cortical Thickness Measurements Across Scanners and Sites." *NeuroImage* 167: 104–120.

Fortin, J.-P., D. Parker, B. Tunç, et al. 2017. "Harmonization of Multi-Site Diffusion Tensor Imaging Data." *NeuroImage* 161: 149–170.

Fotiadis, P., M. Cieslak, X. He, et al. 2023. "Myelination and Excitation-Inhibition Balance Synergistically Shape Structure-Function Coupling Across the Human Cortex." *Nature Communications* 14: 6115.

Fotiadis, P., L. Parkes, K. A. Davis, T. D. Satterthwaite, R. T. Shinohara, and D. S. Bassett. 2024. "Structure–Function Coupling in Macroscale Human Brain Networks." *Nature Reviews. Neuroscience* 25: 688–704.

Frizzell, T. O., M. Glashutter, C. C. Liu, et al. 2022. "Artificial Intelligence in Brain MRI Analysis of Alzheimer's Disease Over the Past 12 Years: A Systematic Review." *Ageing Research Reviews* 77: 101614.

Grieder, M., D. J. J. Wang, T. Dierks, L.-O. Wahlund, and K. Jann. 2018. "Default Mode Network Complexity and Cognitive Decline in Mild Alzheimer's Disease." *Frontiers in Neuroscience* 12: 770.

Gu, Y., Y. Lin, L. Huang, et al. 2020. "Abnormal Dynamic Functional Connectivity in Alzheimer's Disease." *CNS Neuroscience & Therapeutics* 26: 962–971.

Guo, G., H. Wang, D. Bell, Y. Bi, and K. Greer. 2003. "KNN Model-Based Approach in Classification." In *On the Move to Meaningful Internet Systems 2003: CoopIS, DOA, and ODBASE*, edited by R. Meersman, Z. Tari, and D. C. Schmidt, 986–996. Springer Berlin Heidelberg. Lecture Notes in Computer Science 2888.

Honey, C. J., J.-P. Thivierge, and O. Sporns. 2010. "Can Structure Predict Function in the Human Brain? NeuroImage 52." *Computational Models of the Brain* 52: 766–776.

Jack, C. R., J. S. Andrews, T. G. Beach, et al. 2024. "Revised Criteria for Diagnosis and Staging of Alzheimer's Disease: Alzheimer's Association Workgroup." *Alzheimers Dement* 20: 5143–5169.

Jack, C. R., Jr., D. A. Bennett, K. Blennow, et al. 2018. "NIA-AA Research Framework: Toward a Biological Definition of Alzheimer's Disease." *Alzheimer's & Dementia* 14: 535–562.

Jiang, X., Y. Shen, J. Yao, et al. 2019. "Connectome Analysis of Functional and Structural Hemispheric Brain Networks in Major Depressive Disorder." *Translational Psychiatry* 9: 1–12.

Kim, H. 2012. "A Dual-Subsystem Model of the Brain's Default Network: Self-Referential Processing, Memory Retrieval Processes, and Autobiographical Memory Retrieval." *NeuroImage* 61: 966–977.

Lee, P.-L., K.-H. Chou, C.-P. Chung, et al. 2020. "Posterior Cingulate Cortex Network Predicts Alzheimer's Disease Progression." *Frontiers in Aging Neuroscience* 12: 608667. https://doi.org/10.3389/fnagi.2020.608667.

Li, K., Q. Wei, F.-F. Liu, et al. 2018. "Synaptic Dysfunction in Alzheimer's Disease: Aβ, Tau, and Epigenetic Alterations." *Molecular Neurobiology* 55: 3021–3032.

Li, Z., F. Liu, W. Yang, S. Peng, and J. Zhou. 2022. "A Survey of Convolutional Neural Networks: Analysis, Applications, and Prospects." *IEEE Transactions on Neural Networks and Learning Systems* 33: 6999–7019.

Liu, T., L. Wang, D. Suo, et al. 2022. "Resting-State Functional MRI of Healthy Adults: Temporal Dynamic Brain Coactivation Patterns." *Radiology* 304: 624–632.

Liu, T., M. Wang, J. Zhang, et al. 2024. "Brain Network Dynamics in Patients With Single- and Multiple-Domain Amnestic Mild Cognitive Impairment." *Alzheimer's & Dementia* 20: 7657–7674.

Liu, Z.-Q., B. Vázquez-Rodríguez, R. N. Spreng, B. C. Bernhardt, R. F. Betzel, and B. Misic. 2022. "Time-Resolved Structure-Function Coupling in Brain Networks." *Communications Biology* 5: 1–10.

Madhusudhana, G. K., M. B. Sanjaypande, and B. N. Raveesh. 2020. "Early Detection of Parkinson Disease Progression Using Gaussian Naïve Bayes Machine Learning Approach by Identifying Degeneration in Basal Ganglia Regions." *International Journal of Engineering and Advanced Technology* 10: 433–435.

Maitre, M., H. Jeltsch-David, N. G. Okechukwu, C. Klein, C. Patte-Mensah, and A.-G. Mensah-Nyagan. 2023. "Myelin in Alzheimer's Disease: Culprit or Bystander?" *Acta Neuropathologica Communications* 11: 56.

Mirzaei, G., and H. Adeli. 2022. "Machine Learning Techniques for Diagnosis of Alzheimer Disease, Mild Cognitive Disorder, and Other Types of Dementia." *Biomedical Signal Processing and Control* 72: 103293.

Morris, J. C. 1993. "The Clinical Dementia Rating (CDR)." *Neurology* 43: 2412.

Nasrabady, S. E., B. Rizvi, J. E. Goldman, and A. M. Brickman. 2018. "White Matter Changes in Alzheimer's Disease: A Focus on Myelin and Oligodendrocytes." *Acta Neuropathologica Communications* 6: 22.

Núñez, P., J. Poza, C. Gómez, et al. 2021. "Abnormal Meta-State Activation of Dynamic Brain Networks Across the Alzheimer Spectrum." *NeuroImage* 232: 117898.

Palop, J. J., and L. Mucke. 2016. "Network Abnormalities and Interneuron Dysfunction in Alzheimer Disease." *Nature Reviews. Neuroscience* 17: 777–792.

Parmar, A., R. Katariya, and V. Patel. 2019. "A Review on Random Forest: An Ensemble Classifier." In *International Conference on Intelligent Data Communication Technologies and Internet of Things (ICICI) 2018*, edited by J. Hemanth, X. Fernando, P. Lafata, and Z. Baig, 758–763. Springer International Publishing.

Preti, M. G., T. A. Bolton, and D. Van De Ville. 2017. "The Dynamic Functional Connectome: State-of-the-Art and Perspectives." *NeuroImage* 160: 41–54.

Qing, Z., F. Chen, J. Lu, et al. 2021. "Causal Structural Covariance Network Revealing Atrophy Progression in Alzheimer's Disease Continuum." *Human Brain Mapping* 42: 3950–3962.

Rasmussen, J., and H. Langerman. 2019. "Alzheimer's Disease – Why we Need Early Diagnosis." *Degenerative Neurological and Neuromuscular Disease* 9: 123–130.

Schaefer, A., R. Kong, E. M. Gordon, et al. 2018. "Local-Global Parcellation of the Human Cerebral Cortex From Intrinsic Functional Connectivity MRI." *Cerebral Cortex* 28: 3095–3114.

Sun, Y., Q. Yin, R. Fang, et al. 2014. "Disrupted Functional Brain Connectivity and Its Association to Structural Connectivity in Amnestic Mild Cognitive Impairment and Alzheimer's Disease." *PLoS One* 9: e96505.

Terry, R. D., E. Masliah, D. P. Salmon, et al. 1991. "Physical Basis of Cognitive Alterations in Alzheimer's Disease: Synapse Loss Is the Major Correlate of Cognitive Impairment." *Annals of Neurology* 30: 572–580.

Vázquez-Rodríguez, B., L. E. Suárez, R. D. Markello, et al. 2019. "Gradients of Structure–Function Tethering Across Neocortex." *Proceedings of the National Academy of Sciences* 116: 21219–21227.

Wang, F., S.-Y. Ren, J.-F. Chen, et al. 2020. "Myelin Degeneration and Diminished Myelin Renewal Contribute to Age-Related Deficits in Memory." *Nature Neuroscience* 23: 481–486.

Wang, S., J. Rao, Y. Yue, et al. 2021. "Altered Frequency-Dependent Brain Activation and White Matter Integrity Associated With Cognition in Characterizing Preclinical Alzheimer's Disease Stages." *Frontiers in Human Neuroscience* 15: 625232. https://doi.org/10.3389/fnhum.2021.625232.

Wickramasinghe, I., and H. Kalutarage. 2021. "Naive Bayes: Applications, Variations and Vulnerabilities: A Review of Literature With Code Snippets for Implementation." *Soft Computing* 25: 2277–2293.

Wien, M., H. Schwarz, and T. Oelbaum. 2007. "Performance Analysis of SVC." *IEEE Transactions on Circuits and Systems for Video Technology* 17: 1194–1203.

Wu, M., M. Zhang, X. Yin, et al. 2021. "The Role of Pathological Tau in Synaptic Dysfunction in Alzheimer's Diseases." *Translational Neurodegeneration* 10: 45.

Wu, Y., P. Ren, R. Chen, et al. 2022. "Detection of Functional and Structural Brain Alterations in Female Schizophrenia Using Elastic Net Logistic Regression." *Brain Imaging and Behavior* 16: 281–290.

Xiao, R., X. Cui, H. Qiao, et al. 2021. "Early Diagnosis Model of Alzheimer's Disease Based on Sparse Logistic Regression With the Generalized Elastic Net." *Biomedical Signal Processing and Control* 66: 102362.

Zhang, J., Y. Zhang, L. Wang, et al. 2017. "Disrupted Structural and Functional Connectivity Networks in Ischemic Stroke Patients." *Neuroscience* 364: 212–225.

Zhang, Z., H. Zheng, K. Liang, et al. 2015. "Functional Degeneration in Dorsal and Ventral Attention Systems in Amnestic Mild Cognitive Impairment and Alzheimer's Disease: An fMRI Study." *Neuroscience Letters* 585: 160–165.

Zheng, W., B. Cui, Y. Han, et al. 2019. "Disrupted Regional Cerebral Blood Flow, Functional Activity and Connectivity in Alzheimer's Disease: A Combined ASL Perfusion and Resting State fMRI Study." *Frontiers in Neuroscience* 13: 738. https://doi.org/10.3389/fnins.2019.00738.

Zou, H., and T. Hastie. 2005. "Regularization and Variable Selection via the Elastic Net." *Journal of the Royal Statistical Society, Series B: Statistical Methodology* 67: 301–320.

Supporting Information

Additional supporting information can be found online in the Supporting Information section.